ACS APPLIED MATERIALS & INTERFACES

www.acsami.org

Research Article

An Autocatalytic DNA Circuit Based on Hybridization Chain Assembly for Intracellular Imaging of Polynucleotide Kinase

Yushi Wang,[†] Yingying Chen,[†] Yeqing Wan, Chen Hong, Jinhua Shang, Fengzhe Li, Xiaoqing Liu, and Fuan Wang*

Cite This: *ACS Appl. Mater. Interfaces* 2022, 14, 31727−31736

Read Online

ACCESS | Metrics & More | Article Recommendations | Supporting Information

ABSTRACT: Polynucleotide kinase (PNK) plays an essential role in various cellular events by regulating phosphorylation processes, and abnormal homeostasis of PNK could cause many human diseases. Herein, we proposed an autocatalytic hybridization system (AHS) through the elaborate integration of hybridization chain assembly (HCA) and catalytic DNA assembly (CDA) that enables a highly efficient positive feedback amplification. The PNK-targeting AHS biosensor is composed of three modules: a recognition module, an HCA amplification module, and a CDA autocatalytic module. In the presence of PNK, the recognition module could transform the PNK input into an exposed nucleic acid initiator (**I**). Then the initiator strand **I** could trigger the autonomous HCA process in the amplification module, and the resulted HCA products could reassemble the split CDA trigger strand **T**, subsequently inducing the CDA process in the autocatalytic module to form abundant DNA duplex products. Consequently, the embedded initiator strand **I** was liberated from the CDA duplex product to autonomously trigger the new rounds of HCA circuit. The rational integration and cooperative cross-activation between the HCA and CDA module could prominently accelerate the reaction and realize the exponential amplification efficiency by initiator regeneration. As a result, the self-sustainable AHS amplifier could implement the sensitive detection of PNK *in vitro* and in biological samples and further fulfill accurate monitoring of the intracellular PNK activity and the effective screening of PNK inhibitors. This work paves a way for exploiting highly efficient artificial DNA circuits to analyze low-abundance biomarkers, holding great potential in biochemical research and clinical diagnosis.

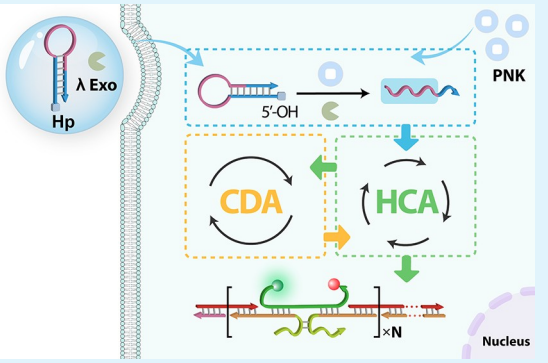

KEYWORDS: *polynucleotide kinase, hybridization, fluorescence, amplification, imaging*

1. INTRODUCTION

Polynucleotide kinase (PNK) as a vital intracellular protein kinase could catalyze the phosphorylation reactions of 5′-hydroxyl termini of DNA/RNA in the presence of adenosine triphosphate (ATP).[1−4] Because of its biological role in regulating phosphorylation processes, PNK has established great significance in various cellular events, including DNA replication, recombination, and repairing.[5,6] Recently, mounting evidence manifests that the abnormal homeostasis of PNK is closely connected to many human diseases,[7,8] which has become a potential biomarker for clinical diagnostics and biomedical research. Conventional methods such as autoradiography,[9] polyacrylamide gel electrophoresis (PAGE),[10,11] and radical isotope ^{32}P-labeling techniques,[12] have already been employed for PNK detection. However, their further applications are immensely hampered because of cumbersome steps, time consumption, and radioactive hazards. Because of its appealing feature on high predictability, programmability, and biocompatibility, DNA is emerging as an ideal component for engineering functional probes to detect biomarkers.[13,14] Various DNA machines have been devised for PNK sensing, including DNA-based switches,[15] motors,[16] and reaction networks.[17] Nevertheless, intracellular visualization of PNK is still restricted on account of the unsatisfactory sensitivity of these DNA machines. Thus, it is imperative to exploit highly sensitive methods for *in vitro* analysis and *in situ* visualization of intracellular PNK.

Isothermal enzyme-free DNA amplification circuits have aroused enormous interest in the detection of biomarkers by virtue of their excellent signal amplification efficiency, such as hybridization chain assembly (HCA),[18−21] entropy-driven catalysis (EDC),[22−24] catalytic DNA assembly (CDA),[25−27] and deoxyribozyme-induced hydrolytic cleavage (DNAzyme).[28−31] Especially, the HCA amplifier presents less signal leakage for sensing purposes and has attracted extensive

Received: May 13, 2022
Accepted: June 21, 2022
Published: July 5, 2022

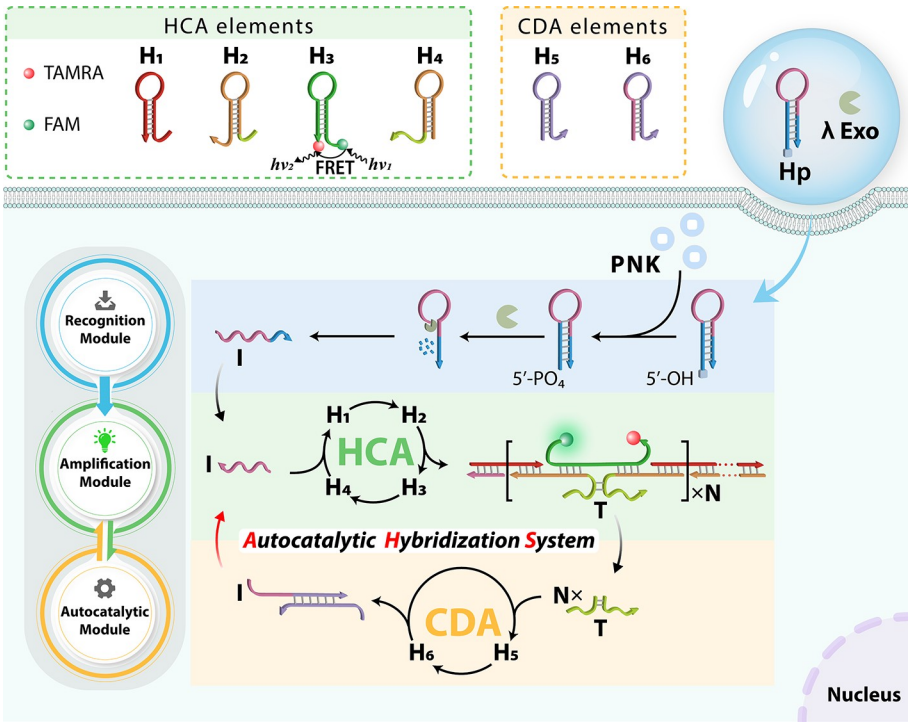

Figure 1. Schematic illustration of autocatalytic hybridization system for detection and imaging of PNK.

attention. In a typical HCA circuit, the target could activate the assembly of the hairpins to form long dsDNA polymers via toehold-mediated strand displacement.[32−35] The HCA circuits are particularly suitable for *in situ* visualization of biomarkers because the as-obtained DNA polymers tethering to initiators could efficiently prevent diffusion of the amplified output signals away from the target sites. To date, a lot of methods based on HCA circuits have been successfully applied in the detection of PNK *in vitro*.[36] However, traditional HCA amplifiers are severely limited by a linear amplification capacity and an insufficient generation of initiators, which is incapable of accomplishing reliable quantification and visualization of PNK. To resolve it, HCA-based cascaded circuits were constructed to satisfy the demands of higher sensitivity by integrating with different amplification circuits.[37] Owing to the endogenous low abundance of PNK, the stacked configuration format still exhibited inadequate signal amplification depth. Positive feedback circuits with exponential dynamics are a promising method for advancing the amplification efficiency, which could achieve the explosive-like autocatalytic generation of the initiator.[38−42] CDA could produce short duplex DNA products,[43−45] where is featured on facile design and rapid reaction kinetics, thus making it an ideal candidate to integrate with the HCA circuit to build an autocatalysis-driven positive feedback system. The initiator-regeneration strategy could improve the biosensing performance, facilitating the development of self-sustainable nucleic acid circuits for *in situ* monitoring intracellular PNK that are still seldom explored.

Herein, we proposed an autocatalytic hybridization system (termed AHS) for the detection and imaging of PNK. The AHS amplifier involved three modules: a recognition module, an amplification module, and an autocatalytic module. The recognition module is aimed to build a bridge between the target analyte PNK and the nucleic acid circuit. A caged probe **Hp** is introduced, which can be phosphorylated by PNK and then disintegrated by λ Exo; thus, the input of PNK can be transformed into an exposed nucleic acid initiator (**I**). Subsequently, in the amplification module, the liberated initiator triggers the isothermal autonomous HCA process, where the hairpins cross-hybridized and produced long duplex DNA assemblies. Note that the HCA products induce the reassembly of the split CDA trigger (**T**), which could lead to stable DNA duplex product via the CDA process in the autocatalytic module. The numerous duplex CDA products liberate abundant HCA initiators that are initially blocked in the CDA hairpin. These newly self-produced HCA initiators can autonomously trigger the new rounds of HCA circuit, leading to highly efficient positive feedback to the HCA amplifier. As a result, the programmed autocatalytic AHS circuit allows the self-sustainable HCA and CDA process to achieve exponential signal amplification, which is expected to fulfill highly sensitive and specific detection of PNK in cell lysates and live cells. Overall, the AHS strategy could offer a promising tool for the detection and *in situ* imaging of low-abundance biomarkers, which possesses considerable prospects for clinical analysis and disease diagnostics.

2. EXPERIMENTAL SECTION

2.1. Materials. All DNA oligonucleotides were synthesized and HPLC purified (Sangon Biotech). The specific sequences of these DNA are provided in Table S1. Polynucleotide kinase (PNK), lambda exonuclease (λ Exo), *Hpa*II, APE1, and CpG methyltransferase (CpG MTase) were obtained from New England BioLabs. Ammonium sulfate ($(NH_4)_2SO_4$), disodium phosphate (Na_2HPO_4), bovine serum albumin (BSA), adenosine triphosphate (ATP), thrombin, and adenosine diphosphate (ADP) were obtained from Sigma-Aldrich.

2.2. Evaluation of PNK Activity and Inhibitor Screening. PNK can catalyze the phosphorylation and degradation reaction of auxiliary probe **Hp** with the assistance of λ Exo. Hairpin **Hp** (4 μM) was heated (95 °C, 5 min) and then cooled to 25 °C for 2 h (fast annealing, in Tris buffer, containing 20 mM Tris, 20 mM $MgCl_2$, pH 8.0). 1 μM **Hp**, 0.2 U/mL λ Exo, and PNK varied from 0 to 2.5 U/mL

https://doi.org/10.1021/acsami.2c08523
ACS Appl. Mater. Interfaces 2022, 14, 31727−31736

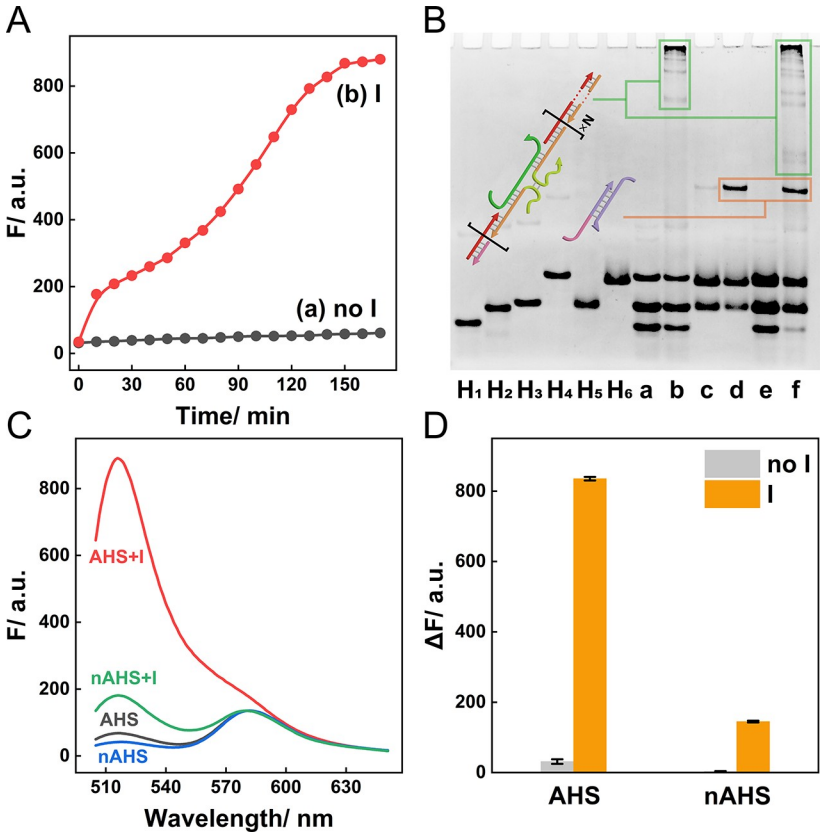

Figure 2. (A) Kinetics of AHS circuit without (curve a) or with (curve b) 20 nM initiator **I** via the fluorescent intensity of FAM fluorophore. (B) Native PAGE characterization of the proposed AHS amplifier: (a) $\mathbf{H_1}$–$\mathbf{H_4}$, (b) $\mathbf{H_1}$–$\mathbf{H_4}$+**I**, (c) $\mathbf{H_5}$–$\mathbf{H_6}$, (d) $\mathbf{H_5}$–$\mathbf{H_6}$+**T**, (e) $\mathbf{H_1}$–$\mathbf{H_6}$, and (f) $\mathbf{H_1}$–$\mathbf{H_6}$+**I**. (C) Fluorescence spectra of the AHS reaction without (curve AHS) or with (curve AHS+**I**) 20 nM initiator **I** and the nAHS system without (curve nAHS) or with (curve nAHS+**I**) 20 nM initiator **I** after 3 h, respectively. (D) Quantified fluorescence intensity variations in (C). Error bars are calculated from the data of three parallel experiments.

were incubated in a buffer (according to the manufacturer's protocol) with addition of 0.05 mM ATP (37 °C, 90 min).

For the PNK inhibitor assay, the AHS system was treated with each inhibitor at different concentrations in the incubation buffer. The relative activity (RA) of PNK was calculated by the equation

$$RA = (F_{inhibitor} - F_{no\ PNK})/(F_{no\ inhibitor} - F_{no\ PNK})$$

where $F_{inhibitor}$ and $F_{no\ inhibitor}$ refer to the fluorescence intensity with and without PNK inhibitor treatment, respectively, and $F_{no\ PNK}$ is the fluorescence intensity without PNK.

2.3. Fluorescence Analysis. Each hairpin probe ($\mathbf{H_1}$–$\mathbf{H_6}$) was diluted to 4 μM in the buffer (10 mM HEPES, 50 mM $MgCl_2$, 1 M NaCl, pH 7.2) and then fast annealed. In the fluorescence assay, the AHS circuit consisted of six hairpin reactants $\mathbf{H_1}$–$\mathbf{H_6}$ (200 nM), the initiator strand **I** (20 nM), or the dual-enzyme-treated auxiliary probe **Hp** (50 nM). The AHS circuit was operated at 25 °C for 3 h. For the assays in the cell lysates, the target PNK was replaced with HeLa cell lysates during the enzyme incubation process. The fluorescence intensity variations (ΔF) were calculated by $\Delta F = F - F_0 = F_{end} - F_{initial}$.

2.4. Polyacrylamide Gel Electrophoresis. In 9% native polyacrylamide gel electrophoresis (PAGE), the concentration of **Hp** was fixed at 1 μM during the PNK recognition module. The AHS circuit was reacted in the buffer consisting of $\mathbf{H_1}$–$\mathbf{H_6}$ (200 nM) and 20 nM initiator **I** (or 50 nM dual-enzyme incubated **Hp**) at 25 °C for 3 h. The GelRed-stained gel was characterized under 365 nm UV irradiation with the aid of FluorChem FC3.

2.5. Intracellular Imaging Experiment. HeLa cells (Human cervical cancer cells, from Shanghai Institutes for Biological Sciences) were plated and then cultured in DMEM (10% FBS, 37 °C, 24 h). The transfection of the PNK-targeting AHS biosensor was performed in two steps. First, **Hp** (100 μM, 1 μL) and λ Exo (5000 U/mL, 2 μL) were transfected into cells for 2 h. Cells were washed with PBS buffer; subsequently, hairpins $\mathbf{H_1}$–$\mathbf{H_6}$ (100 μM each, 1 μL) were incubated with plated cells for 4 h. For the control experiment of the PNK assay, HeLa cells were pretreated with H_2O_2/ADP for 1 h in advance to regulate the PNK activity in live cells. After removal of the incubation medium, the cells were washed with PBS three times. The confocal fluorescence imaging was finally photographed by using a 63× oil-dipping objective by confocal laser scanning microscopy (CLSM, Leica TCS-SP8). All quantitative data of CLSM images were calculated by ImageJ software.

2.6. Flow Cytometry Analysis. Cells were seeded and suspended in 300 μL of PBS after transfection (12-well plates). The flow cytometry measurements were performed by a cytoFLEX system (Beckman Coulter, US). All quantitative calculations of flow cytometry data were operated on FlowJo software.

3. RESULTS AND DISCUSSION

3.1. Principle of the PNK-Targeting AHS Biosensor. To establish a self-sustainable nucleic acid circuit for the sensitive biosensing of PNK, an autocatalytic hybridization system (AHS) was devised as illustrated in Figure 1. The PNK-targeting AHS biosensor contains three parts: a recognition module, an HCA amplification module, and a CDA autocatalytic module. The recognition module could respond to the target PNK. By the sequential PNK-mediated phosphorylation and λ Exo-assisted digestion, the initiator sequence (**I**) could be liberated from the auxiliary probe **Hp**. Thus, the input of PNK can be associated with the HCA amplicon. The HCA amplification module comprised four

https://doi.org/10.1021/acsami.2c08523
ACS Appl. Mater. Interfaces 2022, 14, 31727−31736

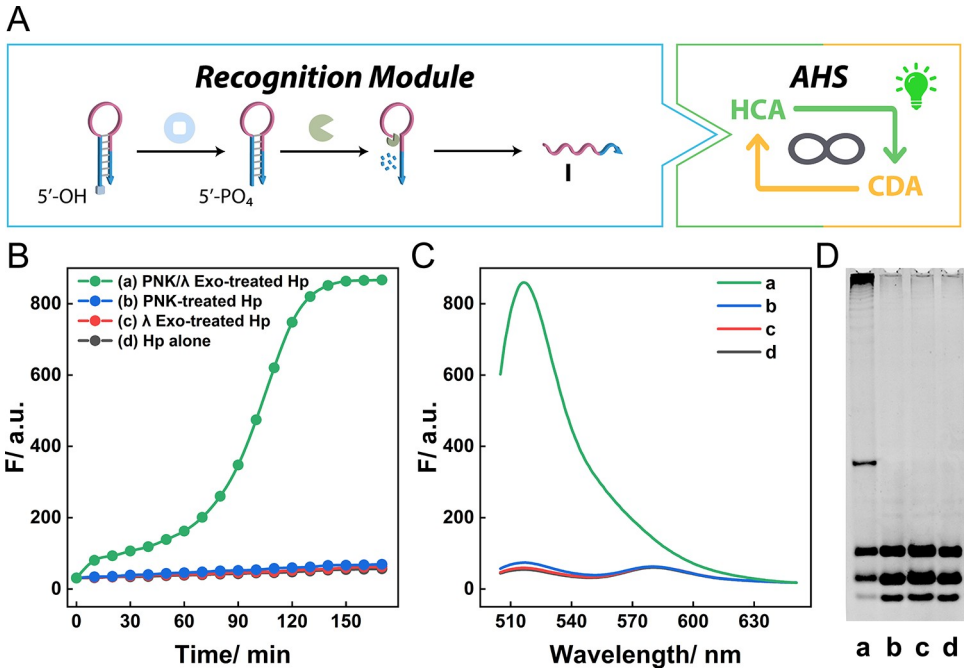

Figure 3. (A) Schematic illustration of the PNK-targeting AHS biosensor. (B) Real-time fluorescence analysis of the AHS-based PNK analysis containing (a) dual PNK/λ Exo-treated **Hp**, (b) PNK-treated **Hp**, (c) λ Exo-treated **Hp**, and (d) **Hp** alone. (C) Fluorescence spectra of the AHS-based PNK analysis after 3 h. (D) Native PAGE analysis.

hairpin probes: $\mathbf{H_1}$, $\mathbf{H_2}$, $\mathbf{H_3}$, and $\mathbf{H_4}$. Of note, the CDA trigger (**T**) was split into two functional units separately connected on hairpins $\mathbf{H_2}$ and $\mathbf{H_4}$. In the amplification module, the exposed initiator (**I**) could hybridize with the toehold domain d of $\mathbf{H_1}$ to form duplex $\mathbf{I}-\mathbf{H_1}$. The unfolded hairpin $\mathbf{H_1}$ thus induced the cross-hybridization of four hairpin probes $\mathbf{H_1}$, $\mathbf{H_2}$, $\mathbf{H_3}$, and $\mathbf{H_4}$ through toehold-mediated strand displacement reaction, ultimately resulting in long dsDNA nanowires $\mathbf{I}-(\mathbf{H_1}\cdot\mathbf{H_2}\cdot\mathbf{H_3}\cdot\mathbf{H_4})_N$ (Figure S1). The HCA products promoted the reassembly of the split CDA trigger (**T**) on hairpins $\mathbf{H_2}$ and $\mathbf{H_4}$, regenerating as domains d-a-b. The downstream CDA autocatalytic module consisted of two hairpins, $\mathbf{H_5}$ and $\mathbf{H_6}$, where the upstream HCA initiator **I** was encoded in hairpin $\mathbf{H_6}$ (Figure S2). Subsequently, numerous reassembled CDA trigger **T** hybridized with toehold d* of hairpin $\mathbf{H_5}$; the newly exposed region b of $\mathbf{H_5}$ then unfolded $\mathbf{H_6}$ via branch migration, causing the continuous assembly of a DNA duplex $\mathbf{H_5}\cdot\mathbf{H_6}$ and the regeneration of countless trigger **T** for CDA. The stable duplex CDA product liberated plenty of initiator **I** sequences, and each copy of **I** could reversely devote to the upstream HCA assembly process, producing continuous positive feedback. Therefore, the elaborately AHS circuit facilitated the production of abundant HCA triggers, which allowed the self-sustainable HCA and CDA processes to accomplish exponential signal amplification. At the same time, fluorophores FAM (as donor) and TAMRA (as acceptor) were modified at 5′ and 3′ termini of $\mathbf{H_3}$, respectively. Initially, the fluorescence of FAM was efficiently quenched by TAMRA through proximity-induced Förster resonance energy transfer (FRET) transduction. Upon the addition of analyte PNK, the continuous assembly of HCA hairpins caused the separation of fluorophore pairs FAM/TAMRA in hairpin $\mathbf{H_3}$; thus, the exponentially amplified "turn-on" signal readouts of fluorophore FAM were collected. This AHS circuit was anticipated to achieve great improvements toward the detection and imaging of low expression level of intracellular PNK.

3.2. Feasibility Analysis of the AHS Circuit. To validate the feasibility of our proposed AHS circuit, a fluorescence assay was conducted under the optimized conditions (Figures S3–S6). As shown in Figure 2A, without the addition of initiator strand **I**, an extremely low fluorescence signal was obtained, indicating that all these involved metastable hairpins could coexist independently without the analyte (curve a). Instead, the incubation of initiator **I** caused intense recovery of FAM fluorescence (λ_{ex} = 488 nm, λ_{em} = 520 nm), continuously increased fluorescence readouts were observed, and the fluorescence intensity reached equilibrium at about 3 h, indicating the autocatalytic hybridization process (curve b).

Native PAGE was further executed to validate the feasibility of the AHS system (Figure 2B). No obvious new band was observed for the mixture of four HCA hairpin reactants in the amplification module (lane a) as well as for the mixture of two CDA hairpin reactants in the autocatalytic module (lane c). In the absence of initiator strand **I**, an almost invisible new band occurred for the AHS circuit (lane e). Thus, the HCA reactants and CDA reactants showed a pretty good non-reacting stability in the AHS system, with exceedingly low background signals, while high-molecular-weight polymerization products were obtained in the HCA process by adding initiator **I** (lane b). Similarly, the CDA process was also activated by trigger **T**, generating a strong band of duplex $\mathbf{H_5}\cdot\mathbf{H_6}$ in lane d. These results demonstrated the successful design of the programmed HCA and CDA circuits. In the integrated AHS circuit, after the addition of initiator **I**, new bands with much lower mobility appeared (lane f), including the HCA and CDA products. As anticipated, the fluorescence and PAGE assays collectively supported the highly efficient operation of the AHS circuit, paving a way for the sensitive analysis of PNK.

Autocatalysis as a kinetic phenomenon often produces sigmoidal intensity–time profiles when the fluorescence intensity of the fluorophore is used to report the product concentration.[46,47] The fluorescence kinetics assay in Figure

https://doi.org/10.1021/acsami.2c08523
ACS Appl. Mater. Interfaces 2022, 14, 31727–31736

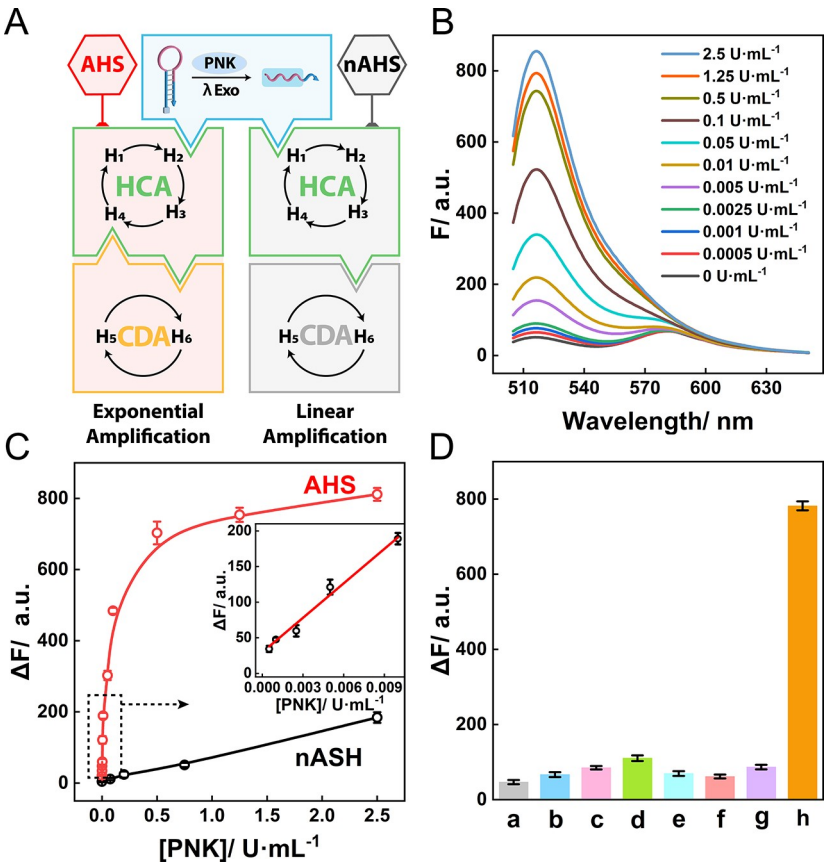

Figure 4. (A) Illustration of the PNK detection with the AHS and nAHS amplified circuit. (B) Fluorescence spectra of the AHS biosensor for analyzing PNK of different concentrations. (C) Calibration curves of the fluorescence intensity change as a function of PNK concentration in the proposed AHS (red curve) and nAHS (black curve) circuit. Inset: the corresponding linear calibration curve of AHS circuit with the concentration of PNK ranges from 0.0025 to 0.125 U/mL. (D) Fluorescence intensity (at λ = 520 nm) of AHS-based PNK biosensor induced by blank control and competing analytes: (a) blank, (b) *Hpa*II, (c) devitalized PNK, (d) BSA, (e) APE1, (f) CpG MTase, (g) thrombin, and (h) PNK. Error bars are calculated from the data of three parallel experiments.

2A indeed confirmed the autocatalytic phenomenon of our AHS circuit. The reaction dynamic was slightly slow initially and then accelerated distinctly with an increase in the product concentration. On the contrary, the fluorescence signal did not exhibit any obvious change without initiator **I** over the same temporal scale.

To further testify the positive-feedback amplification mechanism of the AHS circuit (Figure S7), a nonautocatalytic hybridization system (nAHS) was introduced as the control experiment, where the initiator region in hairpin $\mathbf{H_6}$ was replaced with poly T to inhibit the positive feedback effect of the CDA circuit in autocatalytic module (Figure S8). As a result, the nAHS system could represent the traditional HCA circuit with linear amplification capacity.[48] Upon the addition of initiator strand **I**, the AHS sensor exhibited a dramatically increased fluorescence intensity, while an almost negligible fluorescence signal was obtained for nAHS (Figures 2C, 2D, and S9), thus revealing drastically enhanced signal amplification efficiency of the positive-feedback AHS circuit. In addition, several different hairpin-excluded experiments were also conducted in Figure S10. Only when all hairpin reactants ($\mathbf{H_1}$, $\mathbf{H_2}$, $\mathbf{H_3}$, $\mathbf{H_4}$, $\mathbf{H_5}$, and $\mathbf{H_6}$) were present can the AHS circuit produce a highly amplified FAM signal, implying the indispensable role of each hairpin probe in the smooth operation of the AHS circuit.

3.3. Feasibility Analysis of the PNK-Targeting AHS Biosensor. Next, to test the PNK sensing performance of the AHS biosensor, an auxiliary probe **Hp** was introduced into the recognition module, which was encoded with the sequence of initiator **I** for triggering the HCA circuit (Figure 3A). PNK can catalyze the transfer of phosphate group from the γ-position of ATP to the 5′-hydroxyl termini of **Hp** to make it phosphorylate. The λ Exo can subsequently recognize the 5′-phosphorylated **Hp** and degrade its nucleotides from the double-stranded portion to expose **I**.[49] Without the PNK-assisted 5′-phosphorylation, merely λ Exo cannot cleave probe **Hp** of 5′-hydroxylation. On the basis of this principle, the recognition module can convert the PNK input into the nucleic acid strand **I** to initiate the positive-feedback AHS circuit, thus facilitating the sensitive detection and imaging of PNK.

Both fluorescence and native PAGE assays were utilized to affirm the feasibility of the AHS biosensor for PNK analysis. As expected, an obvious new band was only observed when both PNK and λ Exo were present simultaneously (Figure S11), indicating the collaborative function of these two enzymes for the phosphorylation and cleavage of auxiliary probe **Hp**. Consistently, upon the addition of both PNK and λ Exo, a notable increase in fluorescence signal was attained in Figures 3B and 3C (curve a). The kinetic analysis illustrated that the time-dependent fluorescence enhancement reached saturation

https://doi.org/10.1021/acsami.2c08523
ACS Appl. Mater. Interfaces 2022, 14, 31727−31736

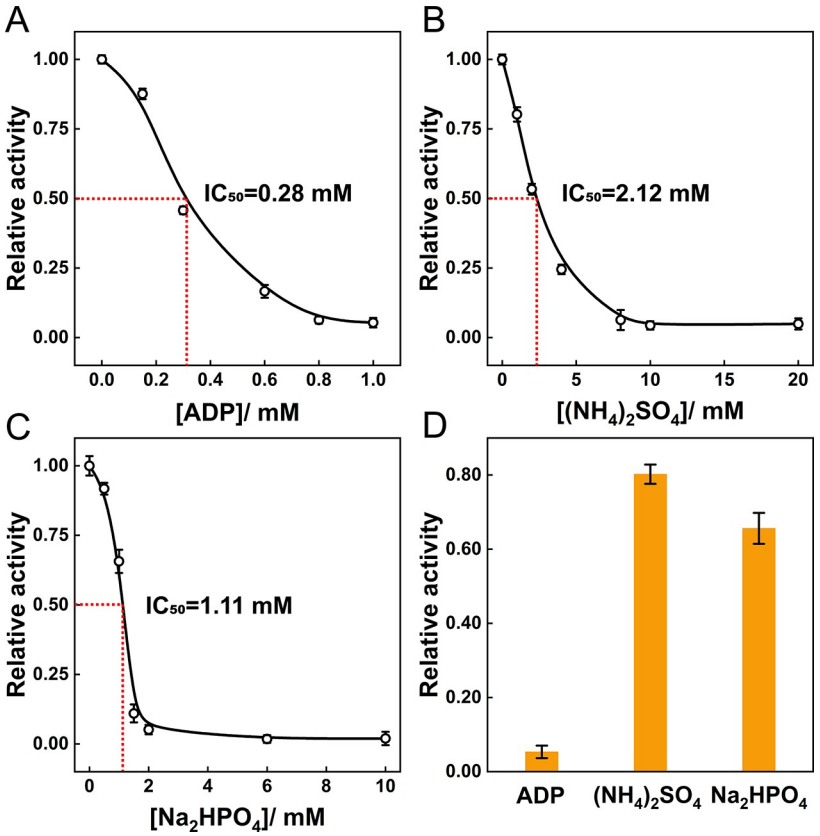

Figure 5. Relative activity of PNK-targeting AHS biosensor as a function of ADP concentrations (A), $(NH_4)_2SO_4$ concentrations (B), and Na_2HPO_4 concentrations (C). (D) Varied inhibitory effects of different PNK inhibitors at 1 mM. Error bars are calculated from the data of three parallel experiments.

within 3 h. Yet hardly discriminable fluorescence signals were captured without PNK or λ Exo over the operating time, as shown in Figures 3B and 3C (curves b−d). Moreover, the native PAGE also displayed distinct new bands for bulky HCA products and CDA duplex products, under the coexistence of PNK and λ Exo (Figure 3D). Collectively, it validated that the phosphorylation and degradation of **Hp** could liberate the initiator **I** to motivate the AHS circuit, laying the foundation for PNK sensing.

3.4. Assessment of the PNK Detection Performance for the AHS Biosensor. To ensure the optimal conditions for PNK detection, the dosages of ATP and λ Exo were carefully optimized as well as the incubation temperature and duration for enzymes PNK and λ Exo (details in Figure S12). Having optimized the operating conditions of the AHS biosensor, PNK detection performance was examined by the fluorescent assay (Figure 4A). As illustrated in Figure 4B, a gradually enhanced fluorescence intensity of FAM was observed in response to continuously increased concentrations of the target PNK, ranging from 0 to 2.5 U/mL. A linear relationship was acquired between the fluorescence intensity values and PNK concentrations from 0.0005 to 0.01 U/mL (R^2 = 0.988, Figure 4C), from which a limit of detection of 2.98×10^{-4} U/mL was calculated (3σ/slope). Because the positive-feedback function was inhibited by replacing the feedback unit with poly T, the nAHS system with linear amplification capacity only achieved a limit of detection of 0.065 U/mL (Table S2). Therefore, the positive-feedback AHS circuit with exponential amplification efficiency possessed higher sensitivity, which was more favorable to the detection and imaging of low expression level of PNK.

Aside from sensitivity, the selectivity of the AHS circuit for PNK detection was also explored by incubating probe **Hp** with the target PNK and a series of interfering proteins (*Hpa*II, devitalized PNK, BSA, APE1, CpG MTase, and thrombin). As revealed in Figure 4D, an obviously increased fluorescence signal was only observed for the active PNK-induced activation of AHS system (sample h). Yet these interfering proteins produced negligible fluorescence signal alteration, which was comparable to the blank control with low fluorescence background (samples a−g). These data supported that the as-designed AHS circuit exhibited a good selectivity to PNK against other interfering proteins.

3.5. Screening of PNK Inhibitors. PNK inhibitors have drawn immense attention due to their vital roles in various biological processes. On the basis of the highly sensitive PNK detection capability of the exponentially amplified AHS biosensor, we further utilized it to screen PNK inhibitors. Three kinds of kinase inhibitors were selected, including ADP, $(NH_4)_2SO_4$, and Na_2HPO_4, which were reported to inhibit PNK by decreasing the affinity between the enzyme and its substrates but have no inhibition effect on λ Exo.[50,51] Not surprisingly, along with the increasing concentration of ADP, the relative activity of PNK drastically decreased. The IC_{50} value of ADP was calculated to be as low as 0.28 mM (Figure 5A). It was envisioned that the PNK-catalyzed phosphorylation process was reversible, and the transfer of the 5′-phosphate group on polynucleotides to ADP to form ATP could also occur in the presence of both high-concentration

https://doi.org/10.1021/acsami.2c08523
ACS Appl. Mater. Interfaces 2022, 14, 31727−31736

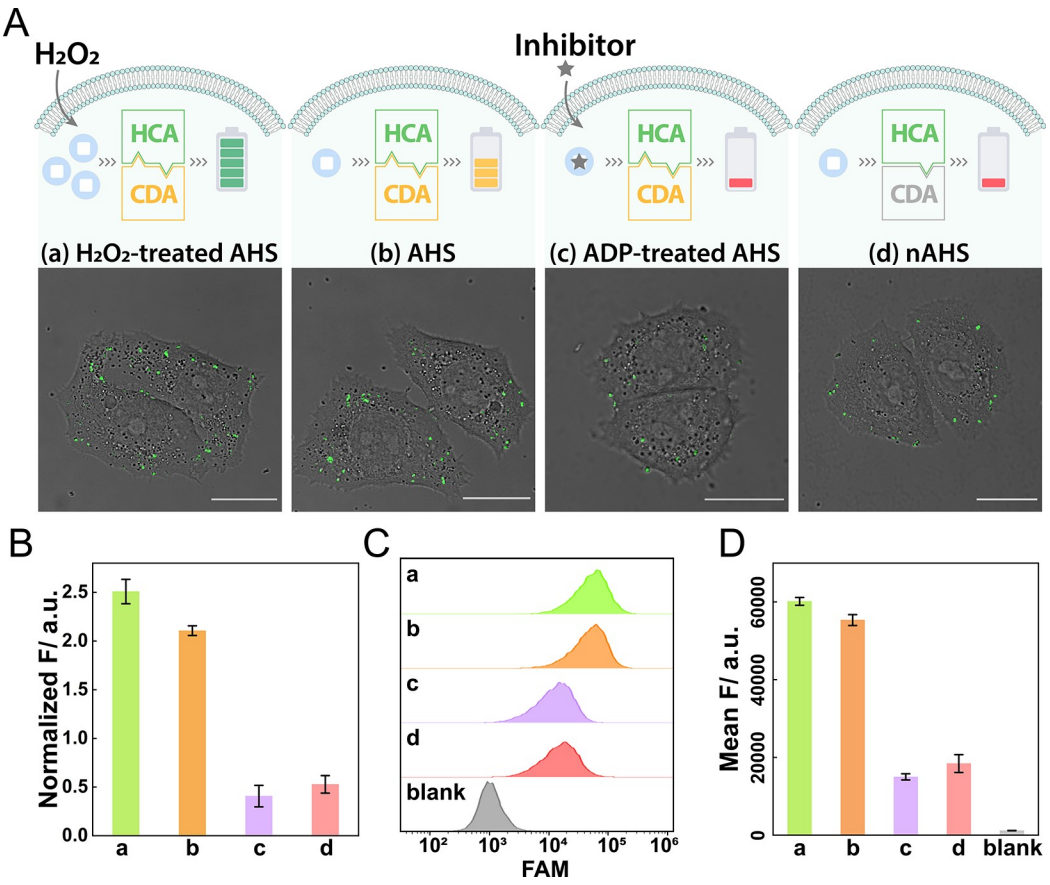

Figure 6. (A) CLSM imaging of PNK by (a) H_2O_2-treated AHS system, (b) AHS system, (c) ADP-treated AHS system, and (d) nAHS system in HeLa cells. Scale bars were 20 μm. (B) Statistical histogram analysis of (A). (C) Flow cytometric assay of HeLa cells incubated with the H_2O_2-treated AHS, AHS, ADP-treated AHS, and nAHS, respectively. (D) Quantification of flow cytometric results in (C). Error bars are calculated from the data of three parallel experiments.

ADP and 5′-phosphorylated DNA. As for Na_2HPO_4 and $(NH_4)_2SO_4$, the IC_{50} values were estimated to be 2.12 and 1.11 mM, respectively (Figures 5B and 5C). These calculated values were comparable to those reported in the literature.[37,50,52] Figure 5D showed the varied inhibitory effects of these above-mentioned three different PNK inhibitors at the same concentration of 1 mM. ADP brought about a more effective inhibition effect on the activity of PNK compared with $(NH_4)_2SO_4$ and Na_2HPO_4. These results conclusively announced that the proposed AHS circuit could be employed as a sensitive tool for the screening of PNK inhibitors, facilitating PNK-related medical research.

3.6. Visualization of PNK in Live Cells. Motivated by the prominent PNK sensing property and good stability of AHS circuit *in vitro* (Figure S13), we sought to assess its performance in complex biological samples, for example, cell lysates. HeLa cells were chosen and lysed. According to Figure S14, a linear correlation was obtained between fluorescence intensity deviation (ΔF) and the dosage of total protein in the range 10−100 ng. The fitting linear equation was $\Delta F = 2.68c + 112$ ($R^2 = 0.992$). These results firmly corroborated the potential of the as-constructed AHS biosensor to analyze PNK in complex samples.

Thanks to the mild reaction conditions and good biocompatibility of the nucleic acid-based AHS circuit, we further evaluated its applicability in live cell imaging. HeLa cells were selected as the model system. The incubation duration of the AHS biosensor was first optimized by flow cytometry analysis. The fluorescence signal of FAM continually accumulated and reached a saturation value at 4 h, which was chosen as the optimal transfection time (Figure S15). The cell imaging was directed by CLSM. To trace the mechanism of the AHS biosensor, the intact AHS system, λ Exo-expelled AHS system, and **Hp**-expelled AHS system were respectively transfected into HeLa cells. According to Figure S16, an appreciable FAM signal was recorded in cells treated with the intact AHS system. As a control, rather faint fluorescent signals were observed in cells treated with the λ Exo- or **Hp**-expelled AHS system. The flow cytometric quantification showed significantly diminished fluorescence signal in HeLa cells by transfecting λ Exo-expelled AHS system and **Hp**-expelled AHS system (Figure S17), which further supported the above cell imaging results. Thus, it was deduced that the successive PNK-mediated phosphorylation and λ Exo-assisted degradation of **Hp** were of fundamental importance to the efficient operation of the functional PNK biosensor.

Next, the AHS biosensor was further extended to monitor the activity of intracellular PNK, based on its high sensitivity for PNK detection. H_2O_2 was used to stimulate HeLa cells to upregulate the expression level of cellular PNK by prompting the breaking of DNA strands.[53,54] Meanwhile, ADP, the above-mentioned PNK inhibitor, was selected to downregulate the activity of PNK through inhibiting the forward phosphorylation reaction. Compared with the intact cells treated with AHS circuit (sample b, Figure 6A), a more intensified fluorescence response was captured in the H_2O_2-motivated

https://doi.org/10.1021/acsami.2c08523
ACS Appl. Mater. Interfaces 2022, 14, 31727−31736

cells (sample a, Figure 6A). Yet a dramatically attenuated fluorescence signal was observed in the ADP-pretreated cells (sample c, Figure 6A). These data conclusively elucidated that the intelligent AHS biosensor could fulfill the sensitive monitoring of PNK.

To validate the superiority of the AHS circuit with exponential amplification capability in imaging low-abundance biomarkers, a nonfeedback nAHS system was applied as a control, which only possessed linear amplification capacity. As anticipated, a much weaker fluorescence signal was obtained in the nAHS circuit-treated cells (sample d, Figure 6A), in sharp contrast with that of the cells treated with the AHS circuit (sample b, Figure 6A). Quantitatively, the fluorescence intensity in cells incubated with AHS circuit was about a 3-fold increase compared to that of the nAHS circuit-treated cells, further highlighting the benefit of the positive-feedback AHS circuit in enhancing the imaging sensitivity (Figure 6B). A flow cytometry assay was also performed on HeLa cells to further support the above cell imaging results. Similarly, the quantitative flow cytometry data from a large population of cells revealed a consistent trend with that observed in CLSM images (Figure 6C, and 6D). Overall, it was supposed that the positive-feedback AHS biosensor could accomplish the robust and sensitive imaging and monitoring of intracellular PNK, compared with the conventional nAHS circuit. Because of its superior exponential amplification capability, the AHS circuit facilitated the potential applications in PNK-related biochemistry research and diagnosis, affording an intelligent platform for the detection and imaging of low-abundance disease biomarkers.

CONCLUSION

In summary, we presented a robust and sensitive positive-feedback AHS biosensor for the biodetection and intracellular imaging of PNK in living cells. The PNK-targeting AHS circuit was established by the rational combination of a recognition module, an HCA amplification module, and a CDA autocatalytic module. With the aid of an auxiliary probe **Hp** and λ Exo, the target PNK as the input could be transformed into an exposed nucleic acid initiator (**I**). Then the initiator strand **I** could trigger the autonomous HCA process in the amplification module, and the resulted HCA products could reassemble the split CDA trigger strand **T**, thus inducing the CDA process in the autocatalytic module to form countless DNA duplex products. Consequently, the embedded initiator strand **I** was liberated from the CDA duplex product to autonomously trigger the new rounds of HCA circuit. The rational integration and cooperative cross-activation between the HCA and CDA module could significantly accelerate the reaction dynamic and improve the amplification efficiency. As a result, the self-sustainable AHS circuit could realize highly sensitive and specific detection and imaging of PNK in cell lysates and live cells and the effective PNK inhibitor screening. This work opened up a new avenue to exploit highly efficient artificial DNA circuits for *in situ* imaging of low-abundance biomarkers, which held broad application prospects in biochemical research and clinical diagnosis.

ASSOCIATED CONTENT

Supporting Information

The Supporting Information is available free of charge at https://pubs.acs.org/doi/10.1021/acsami.2c08523.

DNA sequences, construction of nonautocatalytic hybridization system, optimization of the PNK-targeting AHS biosensor, PNK detection in cell lysates, and controls of the AHS-mediated imaging system (PDF)

AUTHOR INFORMATION

Corresponding Author

Fuan Wang − *College of Chemistry and Molecular Sciences, Wuhan University, Wuhan 430072, P. R. China;* orcid.org/0000-0002-3063-2485; Email: fuanwang@whu.edu.cn

Authors

Yushi Wang − *College of Chemistry and Molecular Sciences, Wuhan University, Wuhan 430072, P. R. China*

Yingying Chen − *College of Chemistry and Molecular Sciences, Wuhan University, Wuhan 430072, P. R. China*

Yeqing Wan − *College of Chemistry and Molecular Sciences, Wuhan University, Wuhan 430072, P. R. China*

Chen Hong − *College of Chemistry and Molecular Sciences, Wuhan University, Wuhan 430072, P. R. China*

Jinhua Shang − *College of Chemistry and Molecular Sciences, Wuhan University, Wuhan 430072, P. R. China*

Fengzhe Li − *College of Chemistry and Molecular Sciences, Wuhan University, Wuhan 430072, P. R. China*

Xiaoqing Liu − *College of Chemistry and Molecular Sciences, Wuhan University, Wuhan 430072, P. R. China;* orcid.org/0000-0002-1309-5454

Complete contact information is available at: https://pubs.acs.org/10.1021/acsami.2c08523

Author Contributions

†Y.W. and Y.C. contributed equally to this paper.

Notes

The authors declare no competing financial interest.

ACKNOWLEDGMENTS

This work was supported by the National Natural Science Foundation of China (21874103 and 22074112), the Fundamental Research Funds for the Central Universities (2042022kf1175), and the Central Funds Guiding the Local Science and Technology Development of Shenzhen (2021Szvup101).

REFERENCES

(1) Richardson, C. C. Phosphorylation of Nucleic Acid by an Enzyme from T4 Bacteriophage-Infected Escherichia Coli. *Proc. Natl. Acad. Sci. U. S. A.* **1965**, *54*, 158−165.

(2) Tahbaz, N.; Subedi, S.; Weinfeld, M. Role of Polynucleotide Kinase/Phosphatase in Mitochondrial DNA Repair. *Nucleic Acids Res.* **2012**, *40*, 3484−3495.

(3) Cui, L.; Li, Y.; Lu, M.; Tang, B.; Zhang, C. An Ultrasensitive Electrochemical Biosensor for Polynucleotide Kinase Assay Based on Gold Nanoparticle-Mediated Lambda Exonuclease Cleavage-induced Signal Amplification. *Biosens. Bioelectron.* **2018**, *99*, 1−7.

(4) Gu, C.; Gai, P.; Han, L.; Yu, W.; Liu, Q.; Li, F. Enzymatic Biofuel Cell-Based Self-Powered Biosensing of Protein Kinase Activity and Inhibition via Thiophosphorylation-Mediated Interface Engineering. *Chem. Commun.* **2018**, *54*, 5438.

(5) Tang, Z.; Wang, K.; Tan, W.; Ma, C.; Li, J.; Liu, L.; Guo, Q.; Meng, X. Real-Time Investigation of Nucleic Acids Phosphorylation Process Using Molecular Beacons. *Nucleic Acids Res.* **2005**, *33*, e97.

(6) Whitehouse, C. J.; Taylor, R. M.; Thistlethwaite, A.; Zhang, H.; Karimi-Busheri, F.; Lasko, D. D.; Weinfeld, M.; Caldecott, K. W.

XRCC1 Stimulates Human Polynucleotide Kinase Activity at Damaged DNA Termini and Accelerates DNA Single-Strand Break Repair. *Cell* **2001**, *104*, 107−117.
(7) Shen, J.; Gilmore, E. C.; Marshall, C. A.; Haddadin, M.; Reynolds, J. J.; Eyaid, W.; Bodell, A.; Barry, B.; Gleason, D.; Allen, K.; Ganesh, V. S.; Chang, B. S.; Grix, A.; Hill, R. S.; Topcu, M.; Caldecott, K. W.; Barkovich, A. J.; Walsh, C. A. Mutations in PNKP Cause Microcephaly, Seizures and Defects in DNA Repair. *Nat. Genet.* **2010**, *42*, 245−249.
(8) Brosh, R. M.; Bohr, V. A. Human Premature Aging, DNA Repair and RecQ Helicases. *Nucleic Acids Res.* **2007**, *35*, 7527−7544.
(9) Rasouli-Nia, A.; Karimi-Busheri, F.; Weinfeld, M. Stable Down-Regulation of Human Polynucleotide Kinase Enhances Spontaneous Mutation Frequency and Sensitizes Cells to Genotoxic Agents. *Proc. Natl. Acad. Sci. U. S. A.* **2004**, *101*, 6905−6910.
(10) Wang, L. K.; Shuman, S. Domain Structure and Mutational Analysis of T4 Polynucleotide Kinase. *J. Biol. Chem.* **2001**, *276*, 26868−26874.
(11) Meijer, M.; Karimi-Busheri, F.; Huang, T. Y.; Weinfeld, M.; Young, D. Pnk1, a DNA Kinase/Phosphatase Required for Normal Response to DNA Damage by γ-Radiation or Camptothecin in Schizosaccharomyces Pombe. *J. Biol. Chem.* **2002**, *277*, 4050−4055.
(12) Wang, L. K.; Shuman, S. Mutational Analysis Defines the 5′-Kinase and 3′-Phosphatase Active Sites of T4 Polynucleotide Kinase. *Nucleic Acids Res.* **2002**, *30*, 1073−1080.
(13) Yue, S.; Li, Y.; Qiao, Z.; Song, W.; Bi, S. Rolling Circle Replication for Biosensing, Bioimaging, and Biomedicine. *Trends Biotechnol.* **2021**, *39*, 1160−1172.
(14) Zhao, Y.; Xiang, J.; Cheng, H.; Liu, X.; Li, F. Flexible Photoelectrochemical Biosensor for Ultrasensitive MicroRNA Detection Based on Concatenated Multiplex Signal Amplification. *Biosens. Bioelectron.* **2021**, *194*, 113581.
(15) He, H.; Leung, K.; Wang, W.; Chan, D. S.; Leung, C.; Ma, D. Label-Free Luminescence Switch-on Detection of T4 Polynucleotide Kinase Activity Using a G-Quadruplex-Selective Probe. *Chem. Commun.* **2014**, *50*, 5313−5315.
(16) Feng, C.; Wang, Z.; Chen, T.; Chen, X.; Mao, D.; Zhao, J.; Li, G. A Dual-Enzyme-Assisted Three-Dimensional DNA Walking Machine Using T4 Polynucleotide Kinase as Activators and Application in Polynucleotide Kinase Assays. *Anal. Chem.* **2018**, *90*, 2810−2815.
(17) Qing, T.; He, X.; He, D.; Ye, X.; Shangguan, J.; Liu, J.; Yuan, B.; Wang, K. Dumbbell DNA-Templated CuNPs as a Nano-Fluorescent Probe for Detection of Enzymes Involved in Ligase-Mediated DNA Repair. *Biosens. Bioelectron.* **2017**, *94*, 456−463.
(18) Gong, X.; Wang, H.; Li, R.; Tan, K.; Wei, J.; Wang, J.; Hong, C.; Shang, J.; Liu, X.; Liu, J.; Wang, F. A Smart Multiantenna Gene Theranostic System Based on the Programmed Assembly of Hypoxia-Related SiRNAs. *Nat. Commun.* **2021**, *12*, 3953.
(19) Liu, X.; Gao, X.; Yang, L.; Zhao, Y.; Li, F. Metal-Organic Framework-Functionalized Paper-Based Electrochemical Biosensor for Ultrasensitive Exosome Assay. *Anal. Chem.* **2021**, *93*, 11792−11799.
(20) Chen, Y.; Gong, X.; Gao, Y.; Shang, Y.; Shang, J.; Yu, S.; Li, R.; He, S.; Liu, X.; Wang, F. Bioorthogonal Regulation of DNA Circuits for Smart Intracellular MicroRNA Imaging. *Chem. Sci.* **2021**, *12*, 15710−15718.
(21) Bi, S.; Yue, S.; Zhang, S. Hybridization Chain Reaction: A Versatile Molecular Tool for Biosensing, Bioimaging, and Biomedicine. *Chem. Soc. Rev.* **2017**, *46*, 4281−4298.
(22) Zhang, D. Y.; Turberfield, A. J.; Yurke, B.; Winfree, E. Engineering Entropy-Driven Reactions and Networks Catalyzed by DNA. *Science* **2007**, *318*, 1121−1125.
(23) Liang, C.; Ma, P.; Liu, H.; Guo, X.; Yin, B.; Ye, B. Rational Engineering of a Dynamic, Entropy-Driven DNA Nanomachine for Intracellular MicroRNA Imaging. *Angew. Chem., Int. Ed.* **2017**, *56*, 9077−9081.
(24) Wu, Y.; Li, Z.; Shi, M.; Yuan, K.; Meng, H.; Qu, L.; Li, Z. Programmable DNAzyme Computing for Specific *In Vivo* Imaging: Intracellular Stimulus-Unlocked Target Sensing and Signal Amplification. *Anal. Chem.* **2021**, *93*, 12456−12463.
(25) Yin, P.; Choi, H. M. T.; Calvert, C. R.; Pierce, N. A. Programming Biomolecular Self-Assembly Pathways. *Nature* **2008**, *451*, 318−322.
(26) Li, X.; Xie, J.; Jiang, B.; Yuan, R.; Xiang, Y. Metallo-Toehold-Activated Catalytic Hairpin Assembly Formation of Three-Way DNAzyme Junctions for Amplified Fluorescent Detection of Hg^{2+}. *ACS Appl. Mater. Interfaces* **2017**, *9*, 5733−5738.
(27) Tang, Y.; Lu, B.; Zhu, Z.; Li, B. Establishment of a Universal and Rational Gene Detection Strategy through Three-Way Junction-Based Remote Transduction. *Chem. Sci.* **2018**, *9*, 760−769.
(28) Wang, Q.; Tan, K.; Wang, H.; Shang, J.; Wan, Y.; Liu, X.; Weng, X.; Wang, F. Orthogonal Demethylase-Activated Deoxyribozyme for Intracellular Imaging and Gene Regulation. *J. Am. Chem. Soc.* **2021**, *143*, 6895−6904.
(29) Hong, C.; Wang, Q.; Chen, Y.; Gao, Y.; Shang, J.; Weng, X.; Liu, X.; Wang, F. Intelligent Demethylase-Driven DNAzyme Sensor for Highly Reliable Metal-Ion Imaging in Living Cells. *Chem. Sci.* **2021**, *12*, 15339−15346.
(30) Wang, F.; Elbaz, J.; Teller, C.; Willner, I. Amplified Detection of DNA through an Autocatalytic and Catabolic DNAzyme-Mediated Process. *Angew. Chem., Int. Ed.* **2011**, *50*, 295−299.
(31) Wang, W.; Satyavolu, N. S. R.; Wu, Z.; Zhang, J.; Zhu, J.; Lu, Y. Near-Infrared Photothermally Activated DNAzyme-Gold Nanoshells for Imaging Metal Ions in Living Cells. *Angew. Chem., Int. Ed.* **2017**, *56*, 6798−6802.
(32) Dirks, R. M.; Pierce, N. A. Triggered Amplification by Hybridization Chain Reaction. *Proc. Natl. Acad. Sci. U. S. A.* **2004**, *101*, 15275−15278.
(33) Li, S.; Li, H.; Li, X.; Zhu, M.; Li, H.; Xia, F. Hybridization Chain Reaction-Amplified Electrochemical DNA-Based Sensors Enable Calibration-Free Measurements of Nucleic Acids Directly in Whole Blood. *Anal. Chem.* **2021**, *93*, 8354−8361.
(34) Yin, Z.; Zhu, L.; Lv, Z.; Li, M.; Tang, D. Persistent Luminescence Nanorods-Based Autofluorescence-Free Biosensor for Prostate-Specific Antigen Detection. *Talanta* **2021**, *233*, 122563.
(35) Gu, C.; Kong, X.; Liu, X.; Gai, P.; Li, F. Enzymatic Biofuel-Cell-Based Self-Powered Biosensor Integrated with DNA Amplification Strategy for Ultrasensitive Detection of Single-Nucleotide Polymorphism. *Anal. Chem.* **2019**, *91*, 8697−8704.
(36) Jie, G.; Li, C.; Zhao, Y.; Kuang, Q.; Niu, S. Fluorescent Mn:ZnCdS@ZnS and CdTe Quantum Dots Probes on SiO_2 Microspheres for Versatile Detection of Carcinoembryonic Antigen and Monitoring T4 Polynucleotide Kinase Activity. *ACS Appl. Nano Mater.* **2019**, *2*, 4637−4645.
(37) Shang, J.; Wei, J.; Wang, Q.; Wang, J.; Zhou, Y.; Yu, S.; Liu, X.; Wang, F. Adaption of an Autonomously Cascade DNA Circuit for Amplified Detection and Intracellular Imaging of Polynucleotide Kinase with Ultralow Background. *Biosens. Bioelectron.* **2020**, *152*, 111994.
(38) Wei, J.; Wang, H.; Wu, Q.; Gong, X.; Ma, K.; Liu, X.; Wang, F. A Smart, Autocatalytic, DNAzyme Biocircuit for *In Vivo*, Amplified, MicroRNA Imaging. *Angew. Chem., Int. Ed.* **2020**, *59*, 5965−5971.
(39) Wan, Y.; Li, G.; Zou, L.; Wang, H.; Wang, Q.; Tan, K.; Liu, X.; Wang, F. A Deoxyribozyme-Initiated Self-Catalytic DNA Machine for Amplified Live-Cell Imaging of MicroRNA. *Anal. Chem.* **2021**, *93*, 11052−11059.
(40) Wei, J.; Wang, H.; Gong, X.; Wang, Q.; Wang, H.; Zhou, Y.; Wang, F. A Proteinase-Free DNA Replication Machinery for *In Vitro* and *In Vivo* Amplified MicroRNA Imaging. *Nucleic Acids Res.* **2020**, *48*, e60.
(41) Yang, J.; Wu, R.; Li, Y.; Wang, Z.; Pan, L.; Zhang, Q.; Lu, Z.; Zhang, C. Entropy-Driven DNA Logic Circuits Regulated by DNAzyme. *Nucleic Acids Res.* **2018**, *46*, 8532−8541.
(42) Zou, L.; Wu, Q.; Zhou, Y.; Gong, X.; Liu, X.; Wang, F. A DNAzyme-Powered Cross-Catalytic Circuit for Amplified Intracellular Imaging. *Chem. Commun.* **2019**, *55*, 6519−6522.

https://doi.org/10.1021/acsami.2c08523
ACS Appl. Mater. Interfaces 2022, 14, 31727−31736

(43) Engelen, W.; Wijnands, S. P. W.; Merkx, M. Accelerating DNA-Based Computing on a Supramolecular Polymer. *J. Am. Chem. Soc.* **2018**, *140*, 9758−9767.
(44) Xing, C.; Dai, J.; Huang, Y.; Lin, Y.; Zhang, K.; Lu, C.; Yang, H. Active Self-Assembly of Train-Shaped DNA Nanostructures via Catalytic Hairpin Assembly Reactions. *Small* **2019**, *15*, 1901795.
(45) Kong, L.; Lv, S.; Qiao, Z.; Yan, Y.; Zhang, J.; Bi, S. Metal-Organic Framework Nanoreactor-Based Electrochemical Biosensor Coupled with Three-Dimensional DNA Walker for Label-Free Detection of MicroRNA. *Biosens. Bioelectron.* **2022**, *207*, 114188.
(46) Widegren, J. A.; Bennett, M. A.; Finke, R. G. Is It Homogeneous or Heterogeneous Catalysis? Identification of Bulk Ruthenium Metal as the True Catalyst in Benzene Hydrogenations Starting with the Monometallic Precursor, Ru(II)(η^6-C_6Me_6)$(OAc)_2$, Plus Kinetic Characterization of the Heterogeneous Nucleation, then Autocatalytic Surface-Growth Mechanism of Metal Film Formation. *J. Am. Chem. Soc.* **2003**, *125*, 10301−10310.
(47) Mondloch, J. E.; Yan, X.; Finke, R. G. Monitoring Supported-Nanocluster Heterogeneous Catalyst Formation: Product and Kinetic Evidence for a 2-Step, Nucleation and Autocatalytic Growth Mechanism of $Pt(0)_n$ Formation from H_2PtCl_6 on Al_2O_3 or TiO_2. *J. Am. Chem. Soc.* **2009**, *131*, 6389−6396.
(48) Wang, H.; He, Y.; Wei, J.; Wang, H.; Ma, K.; Zhou, Y.; Liu, X.; Zhou, X.; Wang, F. Construction of an Autocatalytic Hybridization Assembly Circuit for Amplified *In Vivo* MicroRNA Imaging. *Angew. Chem., Int. Ed.* **2022**, *61*, e202115489.
(49) Hou, T.; Wang, X.; Liu, X.; Lu, T.; Liu, S.; Li, F. Amplified Detection of T4 Polynucleotide Kinase Activity by the Coupled λ Exonuclease Cleavage Reaction and Catalytic Assembly of Bimolecular Beacons. *Anal. Chem.* **2014**, *86*, 884−890.
(50) Jin, T.; Zhang, J.; Zhao, Y.; Huang, X.; Tan, C.; Sun, S.; Tan, Y. Magnetic Bead-Gold Nanoparticle Hybrids Probe Based on Optically Countable Gold Nanoparticles with Dark-Field Microscope for T4 Polynucleotide Kinase Activity Assay. *Biosens. Bioelectron.* **2020**, *150*, 111936.
(51) Zhang, H.; Zhao, Z.; Lei, Z.; Wang, Z. Sensitive Detection of Polynucleotide Kinase Activity by Paper-Based Fluorescence Assay with λ Exonuclease Assistance. *Anal. Chem.* **2016**, *88*, 11358−11363.
(52) Zhou, H.; Luo, R.; Xie, Q.; You, P.; Yu, H.; Qin, Y.; Tong, C.; Danial, M.; Liu, B.; Wang, W. A New Fluorescence Method for Monitoring PNK Activity *In Vitro*, Natural Compounds Screening and Intracellular Imaging. *Sens. Actuators B Chem.* **2021**, *329*, 129203.
(53) Schraufstätter, I.; Hyslop, P. A.; Jackson, J. H.; Cochrane, C. G. Oxidant-Induced DNA Damage of Target Cells. *J. Clin. Invest.* **1988**, *82*, 1040−1050.
(54) Halliwell, B.; Aruoma, O. I. DNA Damage by Oxygen-Derived Species Its Mechanism and Measurement in Mammalian Systems. *FEBS Lett.* **1991**, *281*, 9−19.

https://doi.org/10.1021/acsami.2c08523
ACS Appl. Mater. Interfaces 2022, 14, 31727−31736